# Structural transitions of perylene and coronene on silver and gold surfaces: A molecular-beam epitaxy LEED study

C. Seidel,* R. Ellerbrake, L. Gross, and H. Fuchs

*Physikalisches Institut, Universität Münster, D-48149 Münster, Germany*

(Received 29 November 2000; revised manuscript received 5 April 2001; published 29 October 2001)

The growth of perylene and coronene up to a monolayer is investigated continuously by low-energy electron diffraction (LEED) on the metal surfaces Ag(110), Au(110) $1\times2$, and Au(111) $22\times\sqrt{3}$. Both molecules show [restricted on Au(110) $1\times2$] the evolution from isotropic disordered structure in the submonolayer regime to a highly (substrate-dependent) ordered monolayer. Two-dimensional gas, fluid, and crystalline phases can be distinguished. On the rough Au(110) $1\times2$ surface, a periodic structure in the [001] direction can be observed, while in the [1$\bar{1}$0] direction, diffraction patterns arise from diffuse LEED intensity. Just before the monolayer is complete, structural transitions between highly ordered structures occur in all presented adsorbates. Leaving and reaching of commensurate structures show "stick-slip" behavior. The lateral ordering process of these molecules allows epitaxial growth without domain walls because crystallization does not start from islands in the submonolayer regime.

## I. INTRODUCTION

The adsorption behavior of organic $\pi$-conjugated molecules on single crystals is of great interest because structural and chemical data concerning the monolayer are keys for controlled multilayer growth. Such thin films are interesting for applications like improved electronic and optoelectronic devices. The large variety of organic molecules and functional groups can be used to modify thin-film properties for device optimization. For example, the wavelength of the maximum fluorescence yield can be tailored to the size of the functional group.[1]

Perylene and coronene (structural formula presented in Fig. 1) are rarely used as adsorbates on single crystals in contrast to derivatives like perylene-3,4,9,10-tetracarboxylic-3,4,9,10-dianhydride (PTCDA). This might be due to the fact that coronene and perylene form periodic superstructures on inert surfaces like Ag or Au only at a certain coverage (close to a monolayer) in contrast to most derivatives. Up to a monolayer, all known derivatives form islands in the submonolayer regime. This behavior can be explained by the static electric polarization of these molecules, for example, the quadrupole moment of PTCDA. This static electric moment causes an attractive molecule-molecule interaction explaining this growth mode.

Investigations concerning structural data of pure hydrocarbons were carried out by N. Karl, C. Günther, and U. Zimmermann[2,3] (coronene on MoS$_2$, GeS, and graphite) and by P. Giannoules *et al.*[4,5] [perylene on Ag(111)]. These molecules are much less reactive and can therefore be used as an adsorbate on reactive surfaces like semiconductors. So far, to the best of our knowledge, only one paper exists that shows diffuse low-energy electron-diffraction (LEED) patterns in the submonolayer regime for coronene on graphite and MoS$_2$ (U. Zimmerman and N. Karl[3]) and final superstructures similar to those on Au(111) presented in this work.

Another fundamental motivation is that these molecules can be used as model systems for the basic mechanisms of adsorption, and for lateral ordering processes depending on the binding energy. By observing the adsorption behavior of these molecules the understanding of adsorption processes in general can be improved.

For example, the growing processes of perylene and of the perylene derivative PTCDA on Ag and Au surfaces were compared to find out which parts of the molecules dominate the structural arrangement. Umbach *et al.*[6] found that chemisorption is mainly influenced by the dislocated $\pi$ electrons of PTCDA, the perylene core contributing the majority of these $\pi$ electrons. This view is supported by ultraviolet-photoemission spectroscopy[6,7] and near-edge x-ray-absorption fine-structure[8] investigations made with perylene derivatives on metallic surfaces. Based on this model, a similar adsorption behavior can be expected for perylene; however, this work shows that perylene and PTCDA have very different adsorption behaviors. However, up to now, to the best of our knowledge, no valence-band spectroscopy has been performed on well-defined perylene or coronene monolayers on metallic surfaces.

The two molecules used here differ mainly in size and symmetry because large hydrocarbons with delocalized $\pi$ orbitals should have similar chemical reactivity (converging towards graphite behavior with growing size of the molecules). Therefore, differences in the adsorption geometry and growth mode should show the effects of molecular size and shape on the growth process.

In the present work, we investigated the two similar molecules, perylene and coronene, on three different surfaces [Ag(110), Au(110), and Au(111)]. Structural analyses are based mainly on results from LEED; some are based on scanning tunneling microscopy (STM) investigations. The growth of the molecules was observed continuously from the submonolayer regime up to a monolayer by means of molecular-beam epitaxial (MBE) LEED.[9] Several images were taken to analyze the growth process.

## II. EXPERIMENT

The investigations presented here were obtained in two ultrahigh-vacuum (UHV) chambers. The deposition of coro-
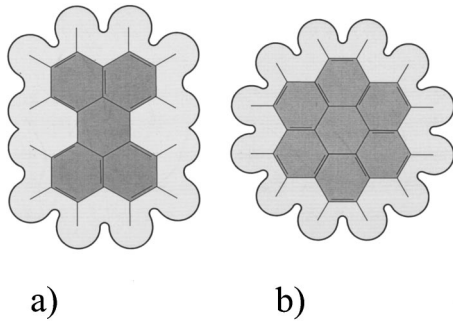
FIG. 1. Molecular structures of (a) a perylene and (b) a coronene molecule with van der Waals radii.
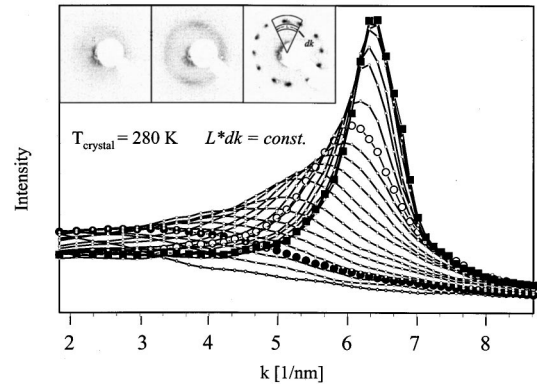


FIG. 2. Normalized electron-diffraction intensity as a function of $k$ vector for perylene on Ag(110). The three diffraction images show the three different states: halo, ring, and spotlike patterns, corresponding to the dotted lines: black circle, white circle, and square, respectively.

nene and perylene and the simultaneous LEED measurements were performed at a residual pressure of 1 $\times 10^{-8}$ Pa. A special MBE LEED (Ref. 9) contains three sublimation cells in which the coronene and perylene crucibles were tilted by 8° and 22° to the surface normal (first UHV chamber). Additional measurements with a variable-temperature STM (Omicron) and a spot profile analysis (SPA) LEED (Omicron) were performed (second UHV chamber). Preparation conditions in the second chamber were similar to those described above. Perylene and coronene were prepared from Knudsen cells either with mass spectrometer control (Balzers QMG 511) or *in situ* at the STM measurement position.

The organic material, which had been purified by a sublimation process, was obtained from W. Schmidt at the Institut für PAH-Forschung, Greifenberg, Germany. The purity and the sublimation rate of the material were checked by the mass spectrometer. Sublimation rates were about 1 ML per min. The substrate was held constant at room temperature during the evaporation process and was not tempered afterwards. We define a monolayer ($\theta = 1$) as the final structure with no change in the positions of the LEED spots at a continuous radiation rate of the molecular beam. Only the signal-noise ratio decreases slightly with increasing background. All the structural transitions presented here occurred up to a saturated (monolayer) coverage, which was partly checked by x-ray photoemission spectroscopy (XPS). Crystal preparation was done as usual by sputtering (500 eV, Ar$^+$ 6 $\mu$A/cm$^2$, 20 min) and heating (up to 700 K) cycles checked by LEED and XPS. The Au(111) surface was checked by LEED with regard to the $23 \times \sqrt{3}$ reconstruction.

## III. RESULTS

### A. Perylene on Ag(110)

Figure 2 shows the normalized ($k^2 = $ constant) diffraction intensity during the growth of perylene on Ag(110) taken at 11 eV as a function of the $k$ value. The other adsorbate systems presented in this paper show a similar behavior [at least in one direction on Au(110) $1 \times 2$]. Starting from an uncovered surface, perylene shows a diffuse LEED pattern like a halo [Fig. 3(a)]. The diffraction intensity is constant up to a $k$ distance of about 3.5 l/nm and lower at higher-$k$ values (Fig. 2, closed-circles line). This halo changes into a ringlike dif-

fuse LEED pattern [Fig. 3(b)], the highest diffraction intensity being concentrated at a $k$ value of 5.7 l/nm (Fig. 2, opened-circles line). At higher coverage (close to a monolayer), this ring decays into single spots [Figs. 3(d)–3(f)], indicating a periodic adsorbate structure. The diffraction pattern reflects the twofold symmetry of the substrate and results from the superposition of two domain orientations. From identification of the first-order diffraction spots and the relation to substrate spots, which were obtained at higher electron energies, the superstructure was derived. The incommensurate final superstructure [Fig. 3(f)] is described by the following matrix notation:

$$\text{perylene} \begin{pmatrix} 3.9 & 0.6 \\ 1 & 2.4 \end{pmatrix} \text{Ag}(110). \tag{1}$$
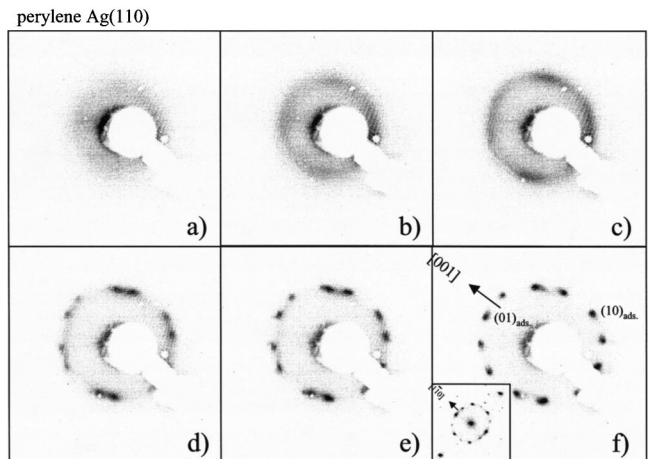
perylene Ag(110)



FIG. 3. LEED images (a)–(f) of perylene on Ag(110) with increasing coverage. First, a diffuse halolike structure occurs (a) that changes to a ringlike structure (b). At higher coverage this ring decays into diffuse spots (c) and finally (d)–(f) into to sharp diffraction pattern, which changes to form the final structure. The inset of (f) represents a SPA-LEED image, which was used for determining the final structure.

$$\begin{pmatrix} 4 & 0.5 \\ 1.5 & 2.5 \end{pmatrix} \qquad \begin{pmatrix} 3.9 & 0.6 \\ 1 & 2.4 \end{pmatrix}$$
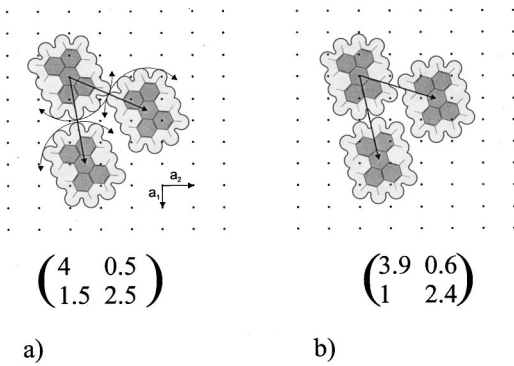
a)                                                 b)

FIG. 4. Real-space configuration of the two perylene superstructures on Ag(110). The unit vectors were obtained from LEED. For this hypothetical model it was assumed that molecules are lying flat without overlap of the van der Waals radii. (a) Intermediate and (b) final superstructure. The curved arrows indicate that molecules can rotate freely.

Here, for obtaining the structural data, we used images of a SPA-LEED optic in which satellite spots allow an accurate determination of the superstructure [Fig. 3(f), inset]. With this equipment, only certain states of film growth could be observed.

The crystallographic data of this and all other adsorbate structures are shown in Table I. Another structure similar to Eq. (1) can be seen as an intermediate state in Figs. 3(d) and 3(e). Its superstructure was analyzed by images of the MBE LEED and is presented by $\begin{pmatrix} 4 & 0.5 \\ 1.5 & 2.5 \end{pmatrix}$. Due to the nature of the superstructures, the molecular density is slightly lower for the intermediate structure [Fig. 4(a)] than for the final structure [Fig. 4(b)]. The real-space model of the structures (Fig. 4) allows the molecules to be parallel ($\pi$ system of the perylene) to the surface without overlap of the van der Waals radii.
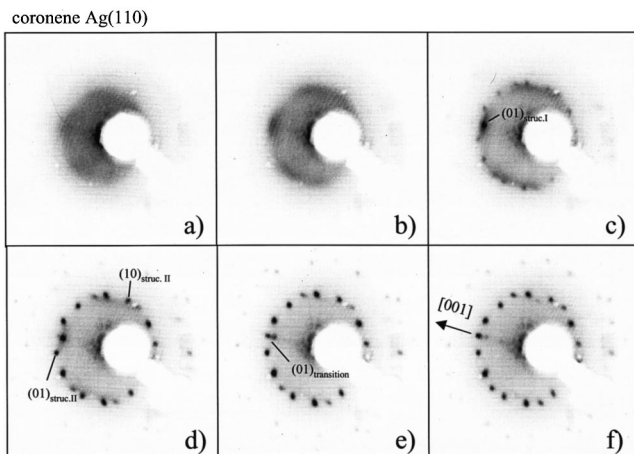


FIG. 5. LEED images (a)–(f) of coronene on Ag(110) with increasing coverage taken at 12 eV. After showing a halolike structure like perylene on Ag(110) (a), a diffuse hexagonal pattern occurs (b), which decays into several spots (c). The pattern contains two different structures, one coexisting with their mirror plane structure. Images (d)–(f) indicate an improved order of the adsorbate and a structural transition of one structure being completed in image (f).



$$\begin{pmatrix} 4 & 0 \\ 2 & 3 \end{pmatrix} \rightarrow \begin{pmatrix} 4 & 0 \\ 2 & 2.5 \end{pmatrix} \qquad \begin{pmatrix} 3 & 2 \\ -1 & 3 \end{pmatrix} \begin{pmatrix} 1 & 3 \\ -3 & 2 \end{pmatrix}$$

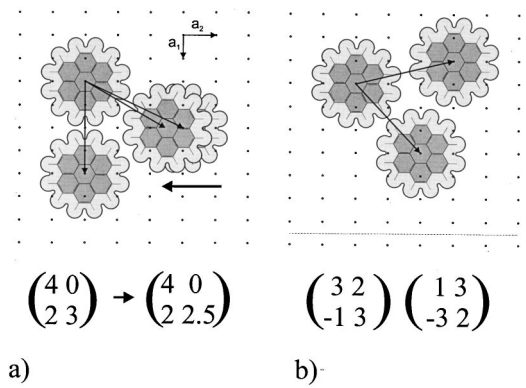a)                                                 b)

FIG. 6. Suggested real-space model for the superstructures of coronene on Ag(110). (a) shows the initial and final states of superstructure I and (b) the incompressible superstructure II reflecting the twofold symmetry of the substrate. The dotted line represents a mirror plane to create the symmetry equivalent structure.

Near the monolayer regime, we found three additional superstructures characterized by LEED and partly by STM. One of these structures is similar to the final structure presented here and can be obtained at higher substrate temperature (about 315 K). The other two structures are totally new structures. They are commensurate but in contrast to the structures described above, the perylene molecules do not lie exactly flat on the substrate surface. We decided not to discuss these structures here as they are very complex and not necessarily relevant to the focus of this paper.

### B. Coronene on Ag(110)

In the extreme submonolayer regime ($\theta \ll 1$), coronene grows on Ag(110) similarly to perylene [Fig. 5(a)]. The diffuse diffraction pattern at this coverage can be described by a halo. At higher coverage, diffraction intensity is mainly concentrated at a $k$ value of 7.7 l/nm in the [001] direction, corresponding to the double of the substrate mesh vector [Figs. 5(b) and 5(c) $(01)_{\text{strud 1}}$]. This diffuse spot becomes sharper at a higher coverage (the nucleus of structure I). Additionally, several other spots occur at nearly the same $k$ distances (Figs. 5(c) and 5(d)). Close to the final state, there is a transition of the spot observed at first to higher-$k$ values [Fig. 5(e)]. The last LEED image shows the final diffraction pattern corresponding to one monolayer, the first-order spots being arranged in a circle. The geometric analysis of these LEED sequences shows that there are two different structures. One of these (structure II) exists in two equivalent domain orientations $\begin{pmatrix} 3 & 2 \\ -1 & 3 \end{pmatrix}$ and $\begin{pmatrix} 1 & 3 \\ -3 & 2 \end{pmatrix}$, being incompressible at a higher molecule dose [Fig. 5(c)]. The other (structure I) occurs only in one domain orientation, and is compressible up to the monolayer structure as described above. The first and final superstructures are specified by $\begin{pmatrix} 4 & 0 \\ 2 & 3 \end{pmatrix}$ and $\begin{pmatrix} 4 & 0 \\ 2 & 2.5 \end{pmatrix}$, respectively. Here, a commensurate coronene structure is transformed into a coincident one. Figure 6 shows that structure I is symmetry equivalent to the substrate [Fig. 6(a)] and that structure II, which exists at least together with its mirror structure [Fig. 6(b)], is incompressible.
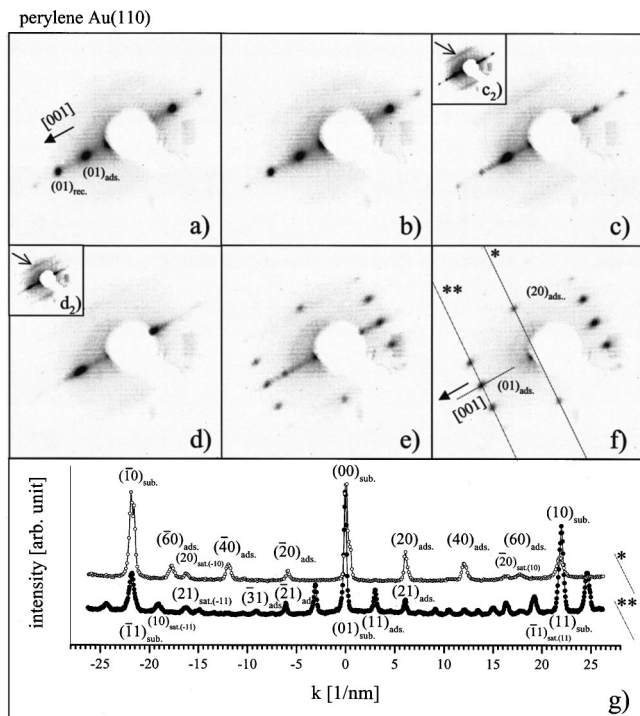
FIG. 7. LEED images (a)–(f) of perylene on Au(110) $1\times2$ with increasing coverage taken at 12 eV. First, an intermediate spot between the $1\times2$ reconstruction spot of the substrate occurs (a). At higher coverage, the substrate spots become weaker, (c) and (d), and a rodlike diffuse diffraction pattern [arrows of the insets (c) and (d)] parallel to the [001] direction appears. The inserts are contrast-enhanced images. Then, the intermediate spot moves to higher-$k$ values (d). Finally, a two-dimensional diffraction pattern forms partly corresponding to the old $1\times2$ periodicity, (e) and (f). The dotted line in (f) (the [001] direction) marks the position of line profiles (see Fig. 8). Two other line profiles obtained by a SPA LEED (taken at 74 eV) are shown in (g). For better orientation, the positions and directions are marked inside the LEED image (f) obtained by the MBE LEED. The SPA LEED resolves up to the (10) substrate spot and shows additional satellite spots, allowing a precise determination of the mesh.

### C. Perylene on Au(110) $1\times2$

The growth of perylene on Au(110) $1\times2$ is shown in Fig. 7 during evaporation. Line profiles in the [001] direction at $k_{[1\bar{1}0]}=0$ from the clean surface up to a complete monolayer are shown in Fig. 8. In the far submonolayer regime [Figs. 7(a) and 8, spectra 1–8], in additional to the reconstruction spots, an intermediate spot at 3.84 l/nm belonging to the perylene superstructure occurs. This is one half of the first-order $1\times2$ reconstruction spot $[(01)_{rec}]$ of the clean Au(110) $1\times2$ surface. Coupled to this, a diffuse rodlike diffraction structure occurs [arrows, Figs. 7(c) (inset) and 7(d) (inset)] expanding with higher coverage from $k_{[1\bar{1}0]}=5.3$ to 6.2 l/nm. This diffuse intensity corresponds to the average distances of the molecules in the $[1\bar{1}0]$ direction (1.19–1.10 nm) arranged like a string of pearls. The structure can be described by the matrix $\begin{pmatrix} X & 0 \\ X & 4 \end{pmatrix}$, with $X$ standing for "undefinable."

At higher coverage (Figs. 7(c), 7(d), and 8, spectra 8–11) the substrate spots $[(01)_{rec}$ and equivalent] become weaker



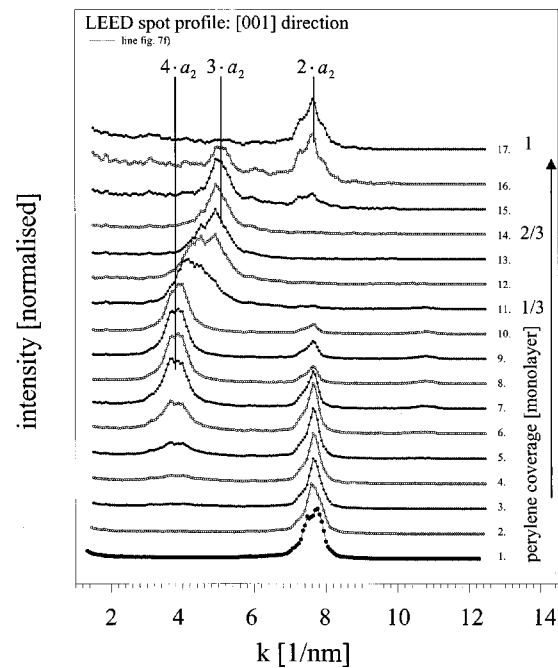FIG. 8. LEED spot profile of 17 steps of perylene preparation on Au(110) $1\times2$ shows the evolution of the central spots in the [001] direction. The spot profiles show four different states. To estimate the degree of coverage in fractions of a monolayer the amount of carbon was investigated by XPS using the C1s signal.

and the diffuse intensity beside the axis [see arrows in Figs. 7(c) (inset) and 7(d) (inset)] decreases slightly while the adsorbate spot $(01)_{ads}$ changes into a $3\times a_2$ (periodic) structure. The transition from the $4\times a_2$ into a $3\times a_2$ structure shows broadening.

At higher coverage the $3\times a_2$ structure disappears (Figs. 7(e) and 8, spectra 17) and a periodic diffraction pattern in two dimensions occurs, which partly fits the original ($1\times2$) row reconstruction of the substrate and can be described by the matrix $\begin{pmatrix} 7.5 & 0 \\ 0 & 2 \end{pmatrix}$ when following LEED and STM analyses. Additional SPA-LEED measurements were carried out to determine the lattice constant $b_1$ [by using substrate (10) and satellite spots] [Fig. 7(g)] with a high precision of 1%. The suppression of the $(10)_{ads}$ spot indicates a superstructure with glide-plane symmetry (the glide plane is parallel to $[1\bar{1}0]$). The line profiles clearly show the suppression of odd values ($x$) of ($x0$) spots obtained by the SPA LEED [Fig. 7(g)]. The dotted line in Fig. 7(f) marks the position of line profiles in the less-resolved image of the standard LEED.

The spectrum suggests at first sight that the spot profile $[(01)_{ads}$, Fig. 8, spectrum 17] of the final structure consists of several peaks; however in view of the limits of the LEED optic (grid structure and partly a moiré structure confined to a resolution of about 0.3 l/nm) this superstructure cannot be interpreted as a property of the sample. Before the final structure is reached, the rodlike diffraction structure [marked with arrows in Figs. 7(c) (inset) and 7(d) (inset)] gets weaker and contracts along the [001] direction to form a sharp spot $[(20)_{ads}]$.
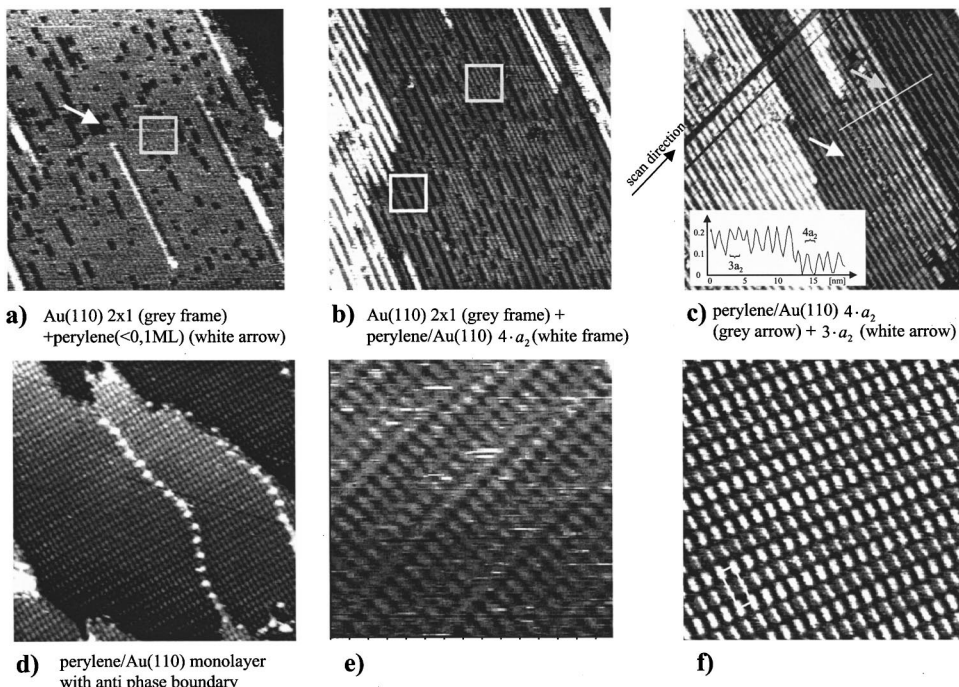
**a)** Au(110) 2x1 (grey frame)
+perylene(<0,1ML) (white arrow)

**b)** Au(110) 2x1 (grey frame) +
perylene/Au(110) 4·$a_2$(white frame)

**c)** perylene/Au(110) 4·$a_2$
(grey arrow) + 3·$a_2$ (white arrow)

**d)** perylene/Au(110) monolayer
with anti phase boundary

**e)**

**f)**

FIG. 9. STM image of four different coverages of perylene on Au(110) $1 \times 2$. Extreme submonolayer (a): perylene occurs as black spots (rows), (b) submonolayer: coexistence of a $4 \times a_2$ perylene structure with an uncovered surface, (c) perylene-covered surface with unresolvable molecules (coexistence of $3 \times a_2$ and $4 \times a_2$ structures), and (d) classical two-dimensional adsorption structure with antiphase domain boundary and an enlargement of one island, (e) and (f). (a)–(d) $45 \times 45$ nm$^2$, (e) and (f) $15 \times 15$ nm$^2$, $U_{tip} = 0.8$ V; $I = 0.1$ nA.

XPS analysis of the $C1s$ signal was done at different coverages to quantify the coverage (see Fig. 8). All the $C1s$ spectra seem to be single peaks without broadening the half width being limited by the pass energy of the electron detector.

Figures 9(a)–9(f) show STM data of the different states. At a coverage far below the submonolayer structure, the undisturbed free Au(110)$1 \times 2$ surface coexists with rows of adsorbed perylene. At higher coverage, these rows form an arealike $4 \times a_2$ structure [Fig. 9(b)], which coexists with the $3 \times a_2$ structure, shown in Fig. 9(c). Only when coverage is close to a complete monolayer do single molecules become visible by STM [Figs. 9(d)–9(f)]. Such STM images show the $p2mg$ superstructure as expected from LEED data as the

first-order $(10)_{ads}$ spot is suppressed. The STM image suggests that the perylene structure can be finally transformed from an incommensurate structure to a coincident one [Fig. 9(e)].

Figure 10 represents the two structures, which were observed as the dominant states received by the LEED and STM measurements. The real-space model [Fig. 10(a)] shows the adsorption according to $4 \times a_2$, with perylene covering only part of the surface. The final structure indicates an overlap of the van der Waals radii if molecules are parallel to the surface.



$$\begin{pmatrix} X & 0 \\ X & 4 \end{pmatrix}$$

a)

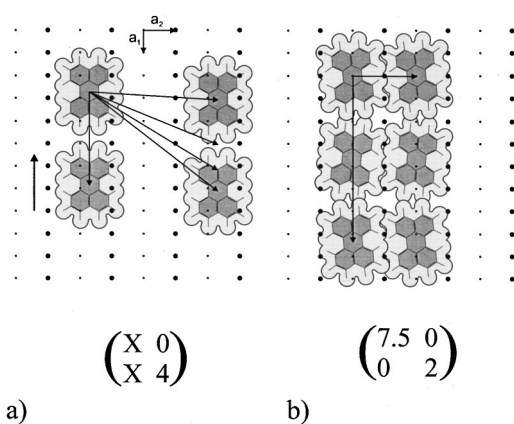$$\begin{pmatrix} 7.5 & 0 \\ 0 & 2 \end{pmatrix}$$

b)

FIG. 10. Real-space model of the first observed $4 \times a_2$ structure (a) and its compression in the $[1\bar{1}0]$ direction and the final structure (b). The unit vectors were obtained from the LEED, SPA-LEED, and STM data; the orientation of the molecules was taken from the STM images.
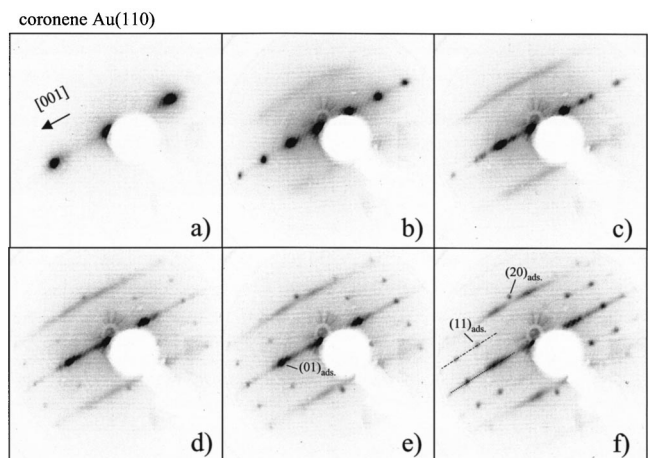


FIG. 11. LEED images (a)–(f) of coronene on Au(110) $1 \times 2$ with increasing coverage, taken at 12 eV. At first, the growing process follows the same pattern as with perylene (a)–(c). Coronene forms a $4 \times 1$ superstructure, which changes to a $3 \times a_2$ at higher coverage, (d) and (e). Image (f) shows a compression of this structure in the $[001]$ direction. The final structure does not fit the original substrate mesh.
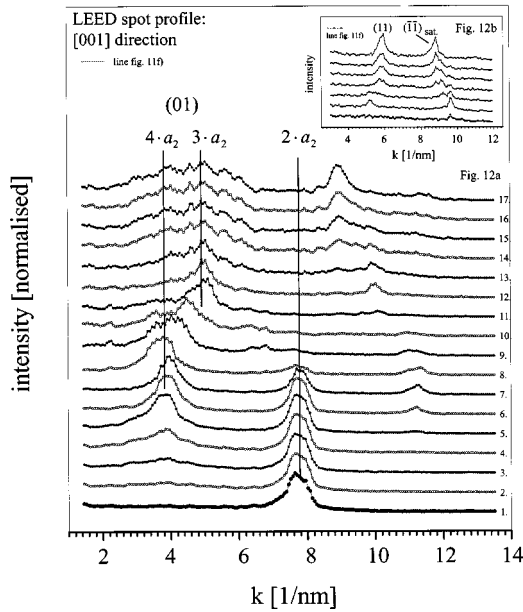
FIG. 12. LEED spot profile of 17 steps of coronene preparation on Au(110) $1\times2$. The evolution of the central spots in the [001] direction is shown. The small frame shows spot profiles of the (11) spot and an (11) satellite in the [001] direction corresponding with the last seven spot profiles of the main spectra and Figs. 11(d)–11(f).

### D. Coronene on Au(110) $1\times2$

At first glance, growth behavior of coronene on Au(110) $1\times2$ [Figs. 11(a)–11(c)] is very similar to that of perylene on Au(110) $1\times2$. At first, coronene forms a $4\times a_2$ structure simultaneously with the original $1\times2$ reconstruction of the Au surface. Then, at higher coverage, these $(1\times2)$ spots disappear. In contrast to what happens in the case of perylene, no spot reappears at this position. Figure 12(a) shows 17 line profiles of the growing process in the [001] direction at $k_{[1\bar{1}0]}=0$ [l/nm]; and additionally, spectra of constant $k_{[1\bar{1}0]}=8.6$ [l/nm] [spot profile of the (11) spot at the surface state according to spectra 12–17] are represented in Fig. 12(b). In this state, as the $3\times a_2$ superstructure emerges (Figs. 11(d) and 12(a), spectra 12), a two-dimensional diffraction pattern according to the matrix $\begin{pmatrix}7.4 & 0\\0 & 3\end{pmatrix}$ appears. This structure shows a continuous compression
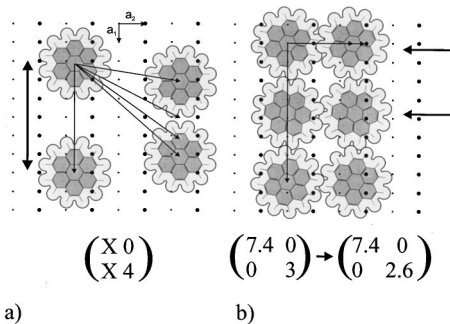


FIG. 13. Real-space model of the first observed $4\times a_2$ structure (a) and the $3\times a_2$ structure (b) that can be compressed to a complete incommensurate final structure $(2.6\times a_2)$.
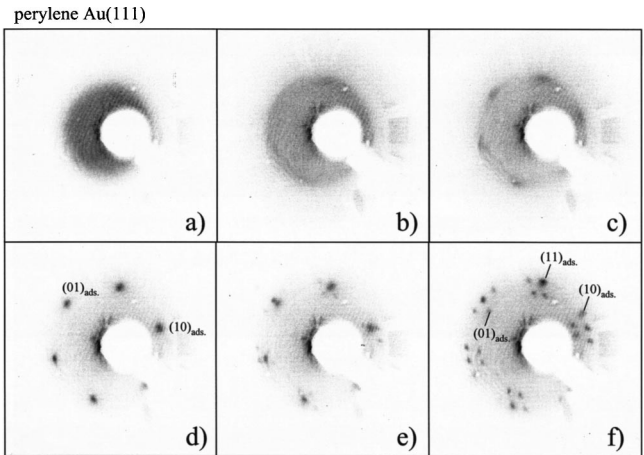


FIG. 14. LEED images (a)–(f) of perylene on Au(111) with increasing coverage taken at 12.9 eV. First, the diffraction pattern is halolike and increases with coverage, (a) and (b). The structure changes from a circlelike shape to a hexagonal shape (b), and diffuse spots at the corners (c). The completely hexagonal structure with low diffuse intensity (d) changes into another structure of lower symmetry, (e) and (f).

along the [001] direction of about 14% resulting in the final structure of $\begin{pmatrix}7.4 & 0\\0 & 2.6\end{pmatrix}$. In comparison to the previous structure, the (01) spots become wider [Fig. 12(a), spectra 14–17]; however, the (11) spot does not show such a behavior [Fig. 11(f)], which suggests that there are additional superstructures in wide distribution. In contrast to the monolayer structure of perylene on Au(110) $1\times2$, the final structure coexists with structures showing diffuse rodlike diffraction patterns. The analyzed final structure does not follow the surface reconstruction pattern at all.

The real-space models in Fig. 13 represent the intermediate $4\times a_2$ superstructure [Fig. 13(a)] and the $3\times a_2$ superstructure [Fig. 13(b)], showing first a two-dimensional LEED pattern with sharp spots, which can be compressed along the [001] direction. The final structure does not allow a molecular arrangement parallel to the surface ($\pi$ system of the perylene), without overlap of the van der Waals radii.

### E. Perylene on Au(111)

The growth of perylene on Au(111) is shown in Figs. 14(a)–14(f). Similar to the growth on Ag(110), there is a halolike diffraction pattern decaying into a ring structure. According to the sixfold symmetry of the substrate, the dif-
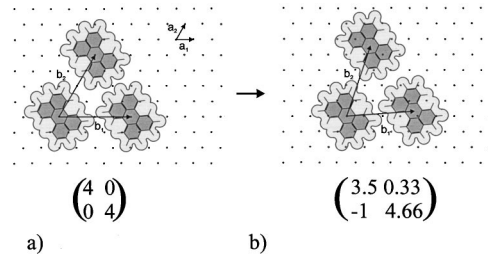


FIG. 15. Suggested real-space model of the $4\times4$ superstructure (a) and the compression into a probably coincident structure (b).
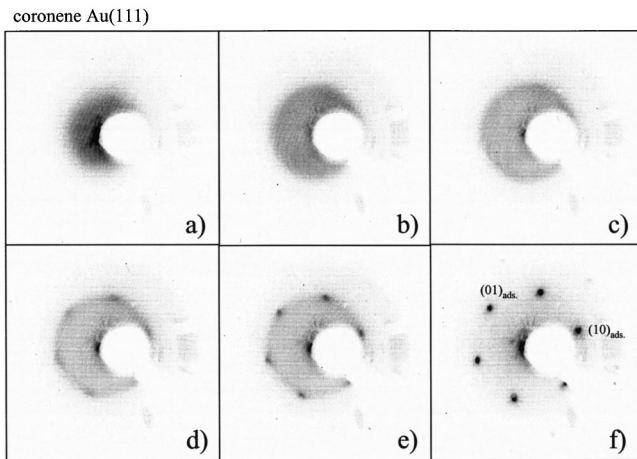
coronene Au(111)



FIG. 16. LEED images (a)–(f) of coronene on Au(111) with increasing coverage taken at 12 eV. First, the diffraction pattern is similar to the growth of perylene (a)–(e). After a hexagonal pattern is complete, the spots move continuously to higher-$k$ values with a low diffuse background up to a certain level of saturation (complete dense monolayer) (f).

fraction pattern [Figs. 13(c)–13(f)] follows this symmetry. This simple hexagonal structure decays into a more complicated structure (the first-order spots are divided into five). After this decay, the structure [Fig. 14(f)] does not change any more during perylene sublimation. This is typical for a saturated monolayer at room temperature and these kind of molecules, indicating a sharp decrease in the sticking coefficient. The superstructure, according to the simple hexagon [Fig. 14(d)], can be described as $\left(\begin{smallmatrix} 4 & 0 \\ 0 & 4 \end{smallmatrix}\right)$ and the final structure [Fig. 14(f)] as $\left(\begin{smallmatrix} 3.5 & 0.33 \\ -1 & 4.66 \end{smallmatrix}\right)$. The intermediate commensurate structure probably changes into a coincident final one, which is shown as a model in Figs. 15(a) and 15(b).
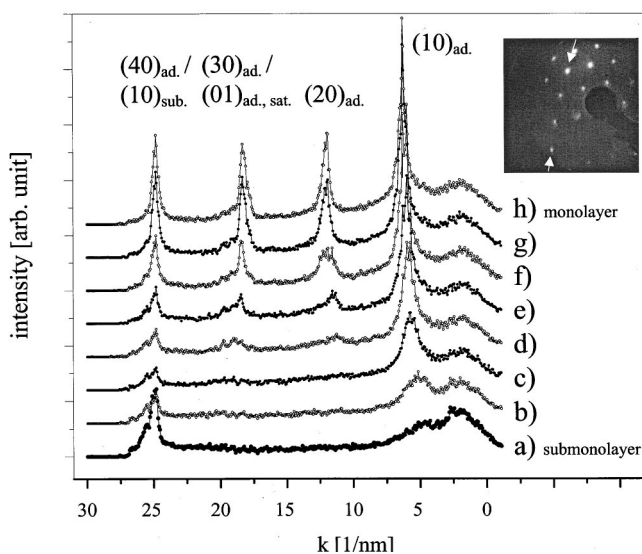


FIG. 17. LEED spot profiles of eight preparation states of coronene on Au(111). The LEED image indicates the position of the line profile. The profile includes the (10)–(40) spots of the adsorbate and additionally a (10) substrate spot.
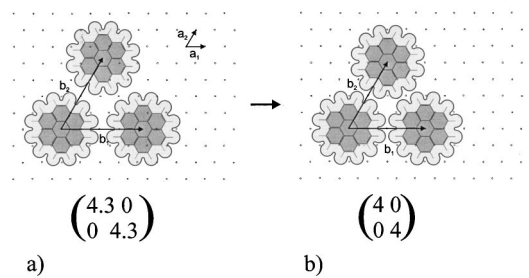


FIG. 18. Suggested real-space model of the $4.3 \times 4.3$ superstructure (a) and the compression into a commensurate structure (b).

### F. Coronene on Au(111)

The last growing process of an organic molecule presented here is coronene on Au(111). It shows three different states represented by their diffraction patterns at room temperature: a diffuse halo [Fig. 16(a)], a diffuse ring structure [Figs. 16(b) and 16(c)] and, finally, sharp diffraction patterns [Figs. 16(d)–16(f)]. After the diffuse diffraction image has become sharp, the hexagonally arranged spots continuously change their spot positions towards higher-$k$ values [Figs. 16(e) and 16(f)]. To relate these slightly changing spots to defined superstructures, diffraction images at higher electron energy were taken. Spot profiles and the LEED image show the range of the spot profile (Fig. 17, white arrows). During this preparation, the sample was tilted against the electron gun to obtain the (10) spot of the Au substrate. This setting allows to distinguish commensurate and coincident/incommensurate structures easily from each other. It is possible that a commensurate structure amplifies the signal intensity of the (10) substrate spots and the adsorbate spots fit into the substrate mesh. The line profiles show that coronene forms a two-dimensional periodic incommensurate structure. At higher coverage, the structure becomes commensurate. The superstructure of the first visible hexagonal structure can be defined as $\left(\begin{smallmatrix} 4.3 & 0 \\ 0 & 4.3 \end{smallmatrix}\right)$ and the final structure as $\left(\begin{smallmatrix} 4 & 0 \\ 0 & 4 \end{smallmatrix}\right)$. This is shown in Fig. 18, where the coronene structure can be compressed without changing the symmetry elements of the whole adsorbate system. On the Au(111) surface showing a $22 \times \sqrt{3}$ reconstruction, no influence of the reconstruction on the superstructures could be observed.

## IV. DISCUSSION

### A. Ordering process

Growing behavior in the monolayer regime depends on adsorbate-substrate and adsorbate-adsorbate interaction. Based on the reactivity of the substrate and the adsorbate, roughly three different types can be distinguished. The combination of a chemically reactive or electrically polar substrate with an adsorbate with similar properties leads to an amorphous growth mirroring the distribution of molecules in the gas phase. For example, PTCDA containing an electrical quadrupole moment adsorbs in an amorphous way on silicon, which is reactive because of its dangling bonds.

During the growing process of PTCDA and 2,9-Dimethylantra [2,1,9-def:6,5,10-d′e′f′]diisoquinoline-1,3,8, 10-tetrone (DMe-PTCDI) on inert metal substrates like silver

TABLE I. Crystallographic data for perylene and coronene on Ag(110), Au(110), and Au(111).

| Adsorbate/substrate superstructure | | $b_1$ (nm) | $b_2$ (nm) | $\Gamma$ (degrees) | $\Phi$ (degrees) | Area (nm$^2$) |
|---|---|---|---|---|---|---|
| **Perylene / Ag(110)** | | | | | | |
| *Intermediate structure* | $\begin{pmatrix} 4 & 0.5 \\ 1.5 & 2.5 \end{pmatrix}$ | 1.17 | 1.11 | 10.0 | 57.0 | 1.09 |
| *Final structure* | $\begin{pmatrix} 3.9 & 0.6 \\ 1 & 2.4 \end{pmatrix}$ | 1.15 | 1.02 | 12.3 | 61.3 | 1.03 |
| **Coronene / Ag(110)** | | | | | | |
| *Intial structure* | $\begin{pmatrix} 4 & 0 \\ 2 & 3 \end{pmatrix}$ | 1.16 | 1.36 | 0 | 64.8 | 1.43 |
| *Compressed intial structure* | $\begin{pmatrix} 4 & 0 \\ 2 & 2.5 \end{pmatrix}$ | 1.16 | 1.17 | 0 | 60.5 | 1.18 |
| | + | | | | | |
| *Structure* II | $\begin{pmatrix} 3 & 2 \\ -1 & 3 \end{pmatrix}$ | 1.19 | 1.26 | 59.9 | 43.3 | 1.03 |
| **Perylene / Au(110) 1×2** | | | | | | |
| *Intermediate structure* | $\begin{pmatrix} X & 0 \\ X & 4 \end{pmatrix}$ | 1.19–1.1 | | 0 | | |
| *Final structure* | $\begin{pmatrix} 7.5 & 0 \\ 0 & 2 \end{pmatrix}$ | 2.16 | 0.82 | 0 | 90 | 1.77 |
| **Coronene / Au(110) 1×2** | | | | | | |
| *Intermediate structure* | $\begin{pmatrix} X & 0 \\ X & 4 \end{pmatrix}$ | | | 0 | | |
| *Intermediate 2d structure* | $\begin{pmatrix} 7.4 & 0 \\ 0 & 3 \end{pmatrix}$ | 2.14 | 1.22 | 0 | 90 | 2.61 |
| *Final structure* | $\begin{pmatrix} 7.4 & 0 \\ 0 & 2.6 \end{pmatrix}$ | 2.14 | 1.06 | 0 | 90 | 2.61 |
| **Perylene / Au(111)** | | | | | | |
| *First structure* | $\begin{pmatrix} 4 & 0 \\ 0 & 4 \end{pmatrix}$ | 1.15 | 1.15 | 0 | 60 | 1.15 |
| *Final structure* | $\begin{pmatrix} 3.5 & 0.33 \\ -1 & 4.66 \end{pmatrix}$ | 1.06 | 1.22 | 4.5 | 67.3 | 1.19 |
| **Coronene / Au(111)** | | | | | | |
| *First structure* | $\begin{pmatrix} 4.3 & 0 \\ 0 & 4.3 \end{pmatrix}$ | 1.24 | 1.24 | 0 | 60 | 1.33 |
| *Final structure* | $\begin{pmatrix} 4 & 0 \\ 0 & 4 \end{pmatrix}$ | 1.15 | 1.15 | 0 | 60 | 1.15 |

and gold, islands of submonolayer coverage were observed,[10] suggesting that the intermolecular force must be attractive and diffusion is not suppressed. For example, the spot profile of an (11) spot is shown in Fig. 19 for DMe-PTCDI on Ag(110).[11] From the submonolayer regime up to a monolayer, no structural transitions are observable with LEED. It can be concluded that during film preparation, the crystalline islands grow laterally without changing their internal structure. This growth mode from nuclei to a mono-layer implies that the formation of domain walls cannot be avoided even if the adsorbate structure completely fits the substrate and shows domains of one orientation only.

The combination of inert organic molecules with inert substrates is investigated in this work. To the best of our knowledge, there are only a few publications describing comparable systems.[2–4,12,13] The typical growth process in Fig. 2 shows a diffuse halo in the submonolayer regime, which, under certain conditions, is transformed into a ring-
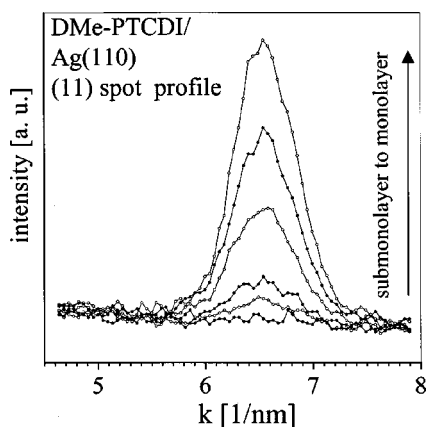
FIG. 19. Spot profile of the (11) spot of DMe-PTCDI on Ag(110) in the $[1\bar{1}0]$ direction. The spot intensity increases monotonically with coverage without changing position. The half width decreases slightly as a function of island size.

like structure and finally, into a common diffraction pattern. An inhomogeneous surface (partly covered with the monolayer structure) was prepared with the system perylene on Ag(110).

After one hour, the diffraction pattern changes to the diffuse ring pattern observed in the submonolayer regime. This proves that there is lateral diffusion (at room temperature, desorption of perylene can be excluded[14]).

Based on these findings we believe that the three different states (diffuse halo, diffuse ring structure, and common diffraction pattern) represent two-dimensional gas, fluid, and crystalline phases. All these structures seem to be thermodynamically controlled showing reversible phase transitions. This contrasts with kinetically controlled ordering like PTDCA/Ag(110), where structures can exist far from the thermodynamic equilibrium.

The structures presented here seem to be controlled mainly by repulsive molecule-molecule interaction. In this work, there is no indication that the attractive part is important for the ordering process.

The same behavior can be observed on Au(110) $1 \times 2$ as well, although restricted to the smooth $[1\bar{1}0]$ direction. The rodlike diffraction pattern belongs to perylene, which is periodically arranged according to the rows of the reconstructed Au surfaces. It can be compressed until repulsive van der Waals interaction of the molecules occurs. In addition to the observed compression as a result of the LEED sequences, STM data obtained from submonolayer films show [Fig. 9(a)] that perylene forms a rodlike structure indicating also an attractive force. The further evolution does not follow a simple scheme. The diffuse LEED intensity becomes weaker, is shortened, and collapses into a sharp spot [Figs. 7(c) (inset), 7(d) (inset), and 7(e)]. According to the STM and LEED evaluations, the final spot belongs to the second order. At this stage, a complicated transition to a $p2mg$ structure occurs, during which the substrate reconstruction probably changes.

### B. Substrate-adsorbate interaction

The substrate-adsorbate interaction is not evaluated quantitatively in this paper. But from differences in the growth

mode with regard to polar derivatives it can be concluded that the interaction of coronene and perylene is quite weak on Ag(110), Au(110), and Au(111) surfaces. The growth mode of PTCDA and DMe-PTCDI on these surfaces seems to be dominated by the polar groups (carboxyl anhydride and the imine group). Coulomb interaction of the charged atoms with the mirror charge of the substrate obviously drives the ordering process and is the dominant factor with regard to binding energy. Thermal-desorption experiments were carried out[14] for perylene on Ag(110). A thermal-desorption signal of the monolayer was found to belong to a desorption energy of 0.5 eV/molecule. Such thermal desorption is not possible with PTCDA. Heating of PTCDA on Ag(111) results in an oxygen-enriched surface, however this is not a proof for a dominant interaction of the $\pi$ system of the perylene core. After dissociation, the perylene core might change the reactivity due to broken bonds.

### C. Structural transitions between periodic structures

Apart from the transitions between diffuse LEED images and common LEED patterns, different kinds of structural transitions between periodic ordered structures are observable. When coverage reaches almost the monolayer regime, a continuous compression of coronene on Au(111) is observed (spot moves continuously towards higher-$k$ values). In contrast to this, the superstructures of coronene on Ag(110) and perylene on Au(111) show an instant compression (a spot becomes weaker at the original position and appears at a new position). These differences may be explained by the difference in the kind of first and final structures. A continuous compression without "stick-slip" behavior is observable if the structure does not pass through an ideal commensurate superstructure state. This demonstrates that diffusion barriers for changing a molecular position are near to the thermal activation energy level.

A different kind of structural transition is observed on the reconstructed Au(110) $1 \times 2$ surface. Here, in the far submonolayer regime, perylene and coronene adsorb along the reconstruction rows although the size of molecules does not fit the row distances. In both cases, the molecules cover every second row of the surface (LEED pattern is like a $4 \times 1$ structure). This behavior can be explained as the row distance of the $1 \times 2$ reconstruction (0.816 nm) is smaller than the size of the molecules. At higher coverage, the adsorbate suppresses the Au reconstruction. In the case of perylene, the final monolayer structure follows again the distance of the rows. Here, molecules seem to be tilted. In the case of coronene, a new superstructure occurs that does not fit the original structure.

### D. Size effect

Comparing the growth of perylene and coronene on the same substrate, the influence of size, shape, and symmetry of the molecules should be observable. We believe that differences in chemical reactivity of coronene and perylene are small except for a scale effect according to the differences in the number of carbon atoms.

For example, on Au(111), perylene and coronene show a $4 \times 4$ superstructure [similar to coronene on Ag(111) that was observed by Giannoules[4]]. This hexagonal superstructure is the final structure for coronene ($D_{6h}$ symmetry) starting from a similar but larger $4.3 \times 4.3$ structure. Also perylene ($D_{2h}$ symmetry) forms a stable hexagonal $4 \times 4$ superstructure on Au(111), which decays into a coincident one at a certain coverage. A possible explanation for this behavior is that a free rotation of the molecules covers up the lower symmetry of the perylene molecule, which forms a hexagonal superstructure. Only at higher coverage is this rotation disturbed and the $4 \times 4$ structure decays into a structure of lower symmetry.

In contrast, a partly commensurate structure on Au(110) was observed for perylene; coronene, however, adsorbs in a totally incommensurate way. Also steric limitation of the molecules defines the structure just before the monolayer is complete. In the case of perylene, molecules seem to be tilted to fit the given substrate distances of $2 \times a_2 (0.816 \text{ nm})$. The coronene structure does not adapt to the substrate structure and creates a similar but larger (than perylene) superstructure.

All high-density structures on Ag(110) and Au(111) surfaces seem to be determined by the shape of the molecules (steric aspects) with the possibility of the substrate influencing the superstructure slightly by a "stick-slip" property. This makes it possible to predict superstructures of similar adsorbate systems, which is impossible for reactive adsorption layers.

## V. CONCLUSION

The investigation shows that perylene and coronene on Ag and Au surfaces behave totally differently from (perylene-based) molecules, which are terminated by polar groups. The differences with regard to the ordering process and the reversibility [perylene/Ag(110)] provide evidence that perylene/coronene does not interact strongly with metals via the $\pi$ system.

Perylene and coronene on Ag(110) and Au(111) show transitions between two-dimensional gas, fluid, and crystalline phases, which are reversible above room temperature. The ordering process, which starts close to a monolayer, makes it possible to create an organic film without domain boundaries, which is totally impossible with superstructures growing from nuclei.

Apart from this, different types of structural transitions were observable. In the case of coronene/Au(111) a commensurate hexagonal final structure exists that grows from an incommensurate one. As opposed to this, at a certain coverage a commensurate structure of perylene on Au(111) decays instantaneously into a coincident one, which exists in different domain orientations.

*Corresponding author. Email address: seidelc@nwz.uni-muenster.de

[1] P. Schouwink, A. H. Schäfer, C. Seidel, and H. Fuchs, Thin Solid Films **372**, 163 (2000).

[2] N. Karl and C. Günther, Cryst. Res. Technol. **34**, 243 (1999).

[3] U. Zimmermann and N. Karl, Surf. Sci. **268**, 296 (1992).

[4] P. Giannoules, Ph.D. thesis, University of Hamburg, 1988.

[5] P. Yannoulis, R. Dudde, K. H. Frank, and E. E. Koch, Surf. Sci. **189/190**, 519 (1987).

[6] E. Umbach, C. Seidel, J. Taborski, R. Li, and A. Soukopp, Phys. Status Solidi B **192**, 389 (1995).

[7] M. Jung, U. Baston, G. Schnitzler, M. Kaiser, J. Papst, T. Porwol, H. J. Freund, and E. Umbach, J. Mol. Struct. **293**, 239 (1993).

[8] J. Taborski, P. Väterlein, H. Dietz, U. Zimmermann, and E. Umbach, J. Electron Spectrosc. Relat. Phenom. **75**, 129 (1995).

[9] C. Seidel, J. Poppensieker, and H. Fuchs, Surf. Sci. **408**, 223 (1998).

[10] K. Glöckler, C. Seidel, A. Soukopp, M. Sokolowski, E. Umbach, M. Böhringer, R. Berndt, and W.-D. Schneider, Surf. Sci. **405**, 1 (1998).

[11] C. Seidel, A. Schäfer, and H. Fuchs, Surf. Sci. **459**, 310 (2000).

[12] N. Karl, K.-H. Kraft, J. Marktanner, M. Münch, F. Schatz, R. Stehle, and H.-M. Uhde, J. Vac. Sci. Technol. A **17**(4), 2318 (1999).

[13] U. Zimmermann, Ph.D. thesis, University of Stuttgart, 1992.

[14] R. Ellerbrake, Ph.D. thesis, University of Münster, 2001.